The final publication is available at

https://doi.org/10.1016/j.euromechsol.2015.03.007

Additional Information

Material-symmetries congruency in transversely isotropic and orthotropic hyperelastic materials

Marcos Latorre, Francisco Javier Montáns*

Escuela Técnica Superior de Ingeniería Aeronáutica y del Espacio
Universidad Politécnica de Madrid
Plaza Cardenal Cisneros, 3, 28040-Madrid, Spain

Abstract

In this work we present the material-symmetries congruency property for anisotropic hyperelastic materials. A transversely isotropic or orthotropic material model holding this property guarantees the recovery of the isotropic behavior when, for example, the volume of reinforcement in a composite material vanishes. A material presenting material-symmetries congruency must show it not only from an analytical, theoretical point of view, but also from a numerical, practical point of view. The former may be obtained from construction of the stored energy function, whereas the latter must be obtained guaranteeing that the parameter-fitting procedure yields material parameters which combined with the specific model results in an isotropic behavior prediction for isotropic materials. We show that some anisotropic models do not present either analytical or numerical material-symmetries congruency.

Keywords: Hyperelasticity, anisotropy, incompressible materials.

---

*Corresponding author. Tel.:+34 637 908 304.
Email addresses: `m.latorre.ferrus@upm.es` (Marcos Latorre),
`fco.montans@upm.es` (Francisco Javier Montáns)

1. Introduction

Many material models have been developed for analyzing hyperelastic transversely isotropic materials and for orthotropic materials, see for example [1–16, 18, 19, 23], among others. The main objective of those material models is to account for different material behavior encountered in different material directions for some materials like rubber [1, 14, 17], fibre-reinforced composites [15, 16] and biological materials [4–13, 18, 19].

The different material properties in the different directions are frequently due to a reinforcing constituent which has some preference in alignment. This reinforcement may be laid-out during manufacturing or, as in biological tissues, by nature. A common approach is to test the composite material as a whole, see for example [12, 17, 23, 24], among others.

Hyperelastic material models typically consist on a stored energy function of some deformation-based invariants [3], some of which are derived from structural tensors obtained from the preferred material directions. These energy functions have a pre-defined shape and some material parameters that are obtained fitting experimental values from some tests using a proper optimization algorithm, typically the Levenberg-Marquardt algorithm, see for example [1, 25] and [26]. Some proposed stored energy functions take into account the fact that anisotropy is mainly due to reinforcement and they separate the stored energy into an isotropic (bulk) part and a reinforcement part, see for example [3, 15, 18]. In fact, these models may include parameters that specifically take into account the amount of anisotropy or reinforcement [3, 15, 16]. Other proposals are more phenomenological and consider from

2

the onset the material as a whole, see for example [1, 2, 19].

Furthermore, in anisotropy it is also frequent to have available less experimental data than those necessary to fully characterize the material [31] and then the missing information may strongly influence the overall behavior [2].

Many of these available constitutive models for transversely isotropic and orthotropic materials intend to represent the behavior of different materials with different degrees of reinforcement, and they intend to do so with parameters obtained from some tests over the composite. One would expect that when the reinforcement volume goes to zero in the composite, the material captures the behavior of the isotropic matrix in an isotropic way. Furthermore, in a orthotropic material, if the reinforcement in one direction vanishes, one would also expect that the model captures the behavior of the transversely isotropic material in a transversely isotropic manner. We say of a model behaving this way that the model has material-symmetries congruency because it converges to an isotropic material when the data corresponds to that of an isotropic material.

The material-symmetries congruency is not only an analytical issue on the form of the stored energy function. A hyperelastic constitutive model may present congruency from an analytical standpoint by construction, but still lack that congruency from a numerical point of view, i.e. the model using the parameters obtained from (quasi-)isotropic experimental curves may not behave in a (quasi-)isotropic manner, simply because the parameter fitting algorithm does not distinguish between quasi isotropic, transversely isotropic and orthotropic materials. Many possible minima can be obtained during the parameter fitting procedure which strongly influence the predicted

behavior even in the isotropic case [26]. In this case, if a model with analytical material-symmetries congruency loses this congruency due to the actual parameters identified from the experiments, we say that whereas the model has analytical material-symmetries congruency, it lacks the numerical one. Material-symmetries congruency is specially important when some experimental data are not available, and also in models that use decompositions of the type of Valanis-Landel [33] because this decomposition has been verified for isotropic materials both experimentally and analytically up to high orders of strain [22], but in general remains to be an assumption on the form of the stored energy for anisotropic materials. If material-symmetries congruency is preserved, only the decomposition on the deviation from isotropy remains as an assumption for moderate large strains. Furthermore, this deviation will tend to vanish in the limit of isotropic behavior.

The purpose of this paper is to present the material-symmetries congruency for anisotropic hyperelastic materials and to analyze some models as examples, both from an analytical perspective and from a numerical one.

2. Theoretical and numerical material-symmetries congruency

Let us define the space $\mathcal{L}$ of the proper orthogonal tensors $\boldsymbol{Q}$

$$\boldsymbol{Q} \in \mathcal{L} \quad / \quad \boldsymbol{Q}\boldsymbol{Q}^T = \boldsymbol{I} \quad \text{and} \quad \det(\boldsymbol{Q}) = 1 \tag{1}$$

and the symmetry group for orthotropic materials $\mathcal{L}_{or} \subset \mathcal{L}$ containing the set of rotation tensors

$$\boldsymbol{Q}_{or} \in \mathcal{L}_{or} = \{\boldsymbol{Q}_{\boldsymbol{a}_0}^{\pi}, \boldsymbol{Q}_{\boldsymbol{b}_0}^{\pi}\} \tag{2}$$

4

where $\boldsymbol{Q}_{\boldsymbol{a}_0}^{\pi} = \boldsymbol{a}_0 \otimes \boldsymbol{a}_0 - \boldsymbol{b}_0 \otimes \boldsymbol{b}_0 - \boldsymbol{c}_0 \otimes \boldsymbol{c}_0$ and $\boldsymbol{Q}_{\boldsymbol{b}_0}^{\pi} = -\boldsymbol{a}_0 \otimes \boldsymbol{a}_0 + \boldsymbol{b}_0 \otimes \boldsymbol{b}_0 - \boldsymbol{c}_0 \otimes \boldsymbol{c}_0$ represent two rotations of π radians around two preferred material directions, defined by the orthogonal vectors $\boldsymbol{a}_0$ and $\boldsymbol{b}_0$. Note that the tensor $\boldsymbol{Q}_{\boldsymbol{c}_0}^{\pi} = \boldsymbol{Q}_{\boldsymbol{a}_0}^{\pi} \boldsymbol{Q}_{\boldsymbol{b}_0}^{\pi}$ associated to the third preferred direction, $\boldsymbol{c}_0 = \boldsymbol{a}_0 \times \boldsymbol{b}_0$, is also included in $\mathcal{L}_{or}$.

For an anisotropic hyperelastic material, in general

$$\mathcal{W}\left(\boldsymbol{E}\right) \neq \mathcal{W}\left(\boldsymbol{Q}\boldsymbol{E}\boldsymbol{Q}^T\right) \tag{3}$$

for a given $\boldsymbol{Q}$ and a Lagrangian strain measure $\boldsymbol{E}$. If the material is orthotropic, it has two (subsequently, three) planes of material symmetry, with $\boldsymbol{a}_0$ and $\boldsymbol{b}_0$ defining these two planes and being perpendicular to them. Then, it can be stated that

$$\mathcal{W}\left(\boldsymbol{E}, \boldsymbol{a}_0, \boldsymbol{b}_0\right) = \mathcal{W}\left(\boldsymbol{Q}_{or}\boldsymbol{E}\boldsymbol{Q}_{or}^T, \boldsymbol{a}_0, \boldsymbol{b}_0\right) \tag{4}$$

where $\boldsymbol{Q}_{or}$ stands now for any arbitrary rotation included in the symmetry group $\mathcal{L}_{or}$. If $\boldsymbol{Q} \notin \mathcal{L}_{or}$, then $\mathcal{W}(\boldsymbol{E}, \boldsymbol{a}_0, \boldsymbol{b}_0) \neq \mathcal{W}(\boldsymbol{Q}\boldsymbol{E}\boldsymbol{Q}^T, \boldsymbol{a}_0, \boldsymbol{b}_0)$ in general. If completely arbitrary rotations $\boldsymbol{Q}$ are considered, this more general invariance relation (i.e. frame independence) is to be fulfilled

$$\mathcal{W}\left(\boldsymbol{E}, \boldsymbol{a}_0, \boldsymbol{b}_0\right) = \mathcal{W}\left(\boldsymbol{Q}\boldsymbol{E}\boldsymbol{Q}^T, \boldsymbol{Q}\boldsymbol{a}_0, \boldsymbol{Q}\boldsymbol{b}_0\right) \tag{5}$$

that is, $\mathcal{W}(\boldsymbol{E}, \boldsymbol{a}_0, \boldsymbol{b}_0)$ must be an isotropic function with respect to its three arguments simultaneously. Note that Eq. (4) stands for symmetry considerations of the strain energy function while Eq. (5) stands for frame indepen-

5

dence so $\mathcal{W}(\boldsymbol{E}, \boldsymbol{a}_0, \boldsymbol{b}_0)$ must satisfy both of them. A material model satisfying only Eq. (5) and not Eq. (4) has not necessarily orthotropic symmetries and it would not be an acceptable formulation for an orthotropic material.

Another property that the function $\mathcal{W}(\boldsymbol{E}, \boldsymbol{a}_0, \boldsymbol{b}_0)$ must obey and which seem to have never been suggested in the literature (to the best of the author's knowledge) is what we call *material-symmetries congruency*. This requirement states that for an orthotropic hyperelastic material, the model being employed should tend to an isotropic formulation when slightly orthotropic, nearly isotropic, materials are being characterized. That is, the tendency of the orthotropic strain energy function when the limit of isotropic behavior is considered should be such that

$$\mathcal{W}\left(\boldsymbol{E}, \boldsymbol{a}_0, \boldsymbol{b}_0\right) \approx \mathcal{W}\left(\boldsymbol{Q}\boldsymbol{E}\boldsymbol{Q}^T, \boldsymbol{a}_0, \boldsymbol{b}_0\right) \tag{6}$$

for *any* proper orthogonal tensor $\boldsymbol{Q}$. Moreover, if an isotropic material is characterized using an orthotropic model, then it is required that

$$\mathcal{W}\left(\boldsymbol{E}, \boldsymbol{a}_0, \boldsymbol{b}_0\right) = \mathcal{W}\left(\boldsymbol{Q}\boldsymbol{E}\boldsymbol{Q}^T, \boldsymbol{a}_0, \boldsymbol{b}_0\right) \tag{7}$$

for any $\boldsymbol{Q}$, as it effectively occurs for isotropic materials, i.e. $\mathcal{W}(\boldsymbol{E}) = \mathcal{W}(\boldsymbol{Q}\boldsymbol{E}\boldsymbol{Q}^T)$. Note the difference between Eq. (4), only required for $\boldsymbol{Q}_{or} \in \mathcal{L}_{or}$, and Eqs. (6) and (7), enforced for arbitrary rotations $\boldsymbol{Q} \in \mathcal{L}$.

We find in the literature some formulations satisfying the requirements given in Eqs. (4) and (5), but which do not fulfill Eqs. (6) and (7) either from a theoretical (e.g. models *SFL* and *TL* in Ref. [12]) or from a, practical, numerical point of view ([1, 18]). For example, consider also the incompressible

uncoupled orthotropic model

$$\mathcal{W}\left(\boldsymbol{E}, \boldsymbol{a}_0, \boldsymbol{b}_0\right) = \omega_{11}\left(E_{11}\right) + \omega_{22}\left(E_{22}\right) + \omega_{33}\left(E_{33}\right)$$
$$+ 2\omega_{12}\left(E_{12}\right) + 2\omega_{23}\left(E_{23}\right) + 2\omega_{31}\left(E_{31}\right) \qquad (8)$$

that we present in Ref. [2]. In Eq. (8), the arguments of the ω functions are the components of the (deviatoric) Hencky strain tensor in the material preferred basis $\boldsymbol{X}_{pr} = \{\boldsymbol{e}_1, \boldsymbol{e}_2, \boldsymbol{e}_3\} = \{\boldsymbol{a}_0, \boldsymbol{b}_0, \boldsymbol{c}_0\}$, that is $E_{ij} = \boldsymbol{e}_i \cdot \boldsymbol{E}\boldsymbol{e}_j$, with $i, j = \{1, 2, 3\}$. Note that these logarithmic strain components are deviatoric (traceless) due to the incompressibility condition, and that the product of the principal stretches is one because of the same reason. Thus, the invariance relation given in Eq. (5) is automatically satisfied and the model is invariant under simultaneous rotations of $\boldsymbol{E}$, $\boldsymbol{a}_0$ and $\boldsymbol{b}_0$. However, note that if any of the shear terms ω_{ij}, $i \neq j$, is not an even function of its corresponding argument E_{ij}, then the model does not satisfy the symmetry requirement of Eq. (4) and the model would not be physically correct. Therefore, we only consider even functions for the shear terms ω_{ij} as we properly address in Ref. [2]. This fact shows that both symmetry and invariance requirements must be satisfied for any orthotropic model and that Eq. (5) is not a sufficient condition for a material model to reproduce an orthotropic behavior.

It can be readily shown that if the orthotropic model of Eq. (8) is used to characterize an assumed symmetric-Valanis-Landel-type incompressible isotropic material from the corresponding set of six different experimental data curves, then the computed model using the procedure detailed in Ref.

[2] reduces to

$$\mathcal{W}\left(\boldsymbol{E}, \boldsymbol{a}_0, \boldsymbol{b}_0\right) = \omega\left(E_{11}\right) + \omega\left(E_{22}\right) + \omega\left(E_{33}\right) + 2\omega\left(E_{12}\right) + 2\omega\left(E_{23}\right) + 2\omega\left(E_{31}\right)$$

(9)

with $\omega\left(E\right)$ being an even function of the strain component E. If as a result of the model determination procedure the function ω contains quadratic terms on its argument, the complete invariant $\boldsymbol{E} : \boldsymbol{E}$ is included in $\mathcal{W}$ multiplied by the proper coefficient (μ), i.e. —E_1, E_2, E_3 represent principal strains

$$\mathcal{W} = \mu E_{11}^2 + \mu E_{22}^2 + \mu E_{33}^2 + 2\mu E_{12}^2 + 2\mu E_{23}^2 + 2\mu E_{31}^2 \tag{10}$$

$$= \mu\left(\boldsymbol{E} : \boldsymbol{E}\right) \tag{11}$$

$$= \mu E_1^2 + \mu E_2^2 + \mu E_3^2 \tag{12}$$

$$= \omega\left(E_1\right) + \omega\left(E_2\right) + \omega\left(E_3\right) \tag{13}$$

and the Valanis–Landel decomposition is recovered in principal directions. On the contrary, if as a result of the model determination procedure the function ω contains fourth-order terms on its argument, the complete invariant $\boldsymbol{E}^2 : \boldsymbol{E}^2$ is not included in $\mathcal{W}$ multiplied by the proper coefficient (μ^*), i.e.

$$\mathcal{W} = (...) + \mu^* E_{11}^4 + \mu^* E_{22}^4 + \mu^* E_{33}^4 + 2\mu^* E_{12}^4 + 2\mu^* E_{23}^4 + 2\mu^* E_{31}^4 \tag{14}$$

$$\neq (...) + \mu^*\left(\boldsymbol{E}^2 : \boldsymbol{E}^2\right) \tag{15}$$

$$= (...) + \mu^* E_1^4 + \mu^* E_2^4 + \mu^* E_3^4 \tag{16}$$

$$= \omega\left(E_1\right) + \omega\left(E_2\right) + \omega\left(E_3\right) \tag{17}$$

so Eq. (7) does not hold. Hence, although an arbitrary strain energy for an orthotropic material can be approximated as closely as desired by a suitable polynomial of the corresponding symmetry-preserving invariants (cf. Ref. [22], pages 211–212), we remark that this "suitable" polynomial should contain the isotropic formulation for the corresponding limit.

Regarding the previous formulation, a possibility to modify the model to obtain theoretical material-symmetries congruency simply consists in adding an isotropic contribution to the orthotropic one

$$\mathcal{W}\left(\boldsymbol{E}, \boldsymbol{a}_0, \boldsymbol{b}_0\right) = \mathcal{W}_{is}\left(\boldsymbol{E}\right) + \mathcal{W}_{or}\left(\boldsymbol{E}, \boldsymbol{a}_0, \boldsymbol{b}_0\right) \tag{18}$$

where $\mathcal{W}_{is}\left(\boldsymbol{E}\right)$ is the Valanis-Landel-type isotropic model expressed in terms of principal logarithmic strains defined by Sussman and Bathe in Ref. [20], i.e.

$$\mathcal{W}_{is}\left(\boldsymbol{E}\right) = \omega\left(E_1\right) + \omega\left(E_2\right) + \omega\left(E_3\right) \tag{19}$$

and $\mathcal{W}_{or}\left(\boldsymbol{E}, \boldsymbol{a}_0, \boldsymbol{b}_0\right)$ is given by Eq. (8). With respect to the modified model provided in Eq. (18), the material-symmetries congruency requirements Eqs. (6) and (7) will be effectively satisfied if both $\mathcal{W}_{or}\left(\boldsymbol{E}, \boldsymbol{a}_0, \boldsymbol{b}_0\right)$ tends to vanish when slightly orthotropic, nearly isotropic, materials are characterized and $\mathcal{W}_{or}\left(\boldsymbol{E}, \boldsymbol{a}_0, \boldsymbol{b}_0\right) = 0$ in the limit of pure isotropic behavior, respectively. In this case, due to the use of the spline-based methodology and the inversion formula (cf. Refs. [2, 19, 20]), the equilibrium equations of the tests are solved exactly for the isotropic model. This important fact implies that $\mathcal{W}_{is}\left(\boldsymbol{E}\right)$ exactly reproduces the prescribed isotropic behavior and that, as a consequence, $\mathcal{W}_{or}\left(\boldsymbol{E}, \boldsymbol{a}_0, \boldsymbol{b}_0\right)$ vanishes for these type of materials.

3. Examples

3.1. Spline-based model according to Latorre and Montáns [19]

In Ref. [19] we present a spline-based transversely isotropic model which is capable of reproducing the uniaxial experimental data of Diani et al. [23] over transversely isotropic calendered rubber with a very good (exact in practice) agreement. In that work, we also compare the results obtained with our model to those predicted by the model of Itskov and Aksel [1], showing a better accuracy achieved by the spline model. Following similar reasonings to those detailed above, it is readily shown that the spline-based model that we presented in Ref. [19] does not have isotropic material-symmetry congruency. However, as mentioned above, the addition of the isotropic contribution of Eq. (19) circumvents this issue.

In this example, and the next ones, we study limit cases in which the two curves presented by Diani et al coalesce to one of both curves. The aim of these examples is to predict with transversely isotropic models some possible isotropic behaviors obtained as isotropic limits of a transversely isotropic material and analyze the numerical material-symmetries congruency of the models. Since the uniaxial tests are performed on an initially *assumed* transversely isotropic material and along its "preferred" material directions, no shear terms are needed and the extended spline-based transversely isotropic model of Ref. [19] reduces to

$$\mathcal{W}\left(\boldsymbol{E}, \boldsymbol{a}_0\right) = \mathcal{W}_{is}\left(\boldsymbol{E}\right) + \mathcal{W}_{tr}\left(\boldsymbol{E}, \boldsymbol{a}_0\right) \tag{20}$$

$$= \omega_1^{\#}\left(E_1\right) + \omega_1^{\#}\left(E_2\right) + \omega_3^{\#}\left(E_3\right) \tag{21}$$
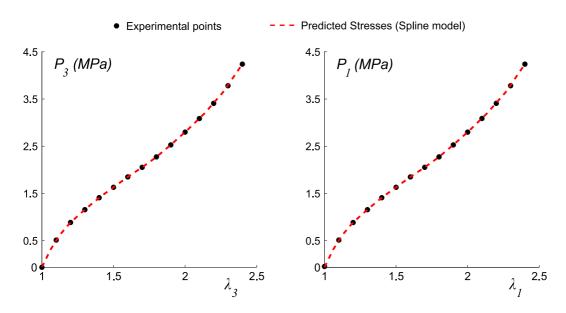
Figure 1: Nominal stresses P_3 and P_1 in terms of the stretches λ_3 and λ_1, respectively, from both uniaxial tests (black solid dots) performed on a transversely isotropic material in a hypothetical limit of isotropic behavior and predictions obtained with the spline-based model. Original experimental data is obtained from the test in calendering direction from Diani et al [23].

where the simplifications $\omega_n^\#(E) = \omega(E) + \omega_n(E)$, $n = 1, 3$, are considered for practical purposes. As in Ref. [19], the subscripts 1 and 2 are associated to two orthogonal directions within the isotropic plane and the subscript 3 represents the assumed preferred direction of the material.

For the first case, we prescribe two discrete stress-stretch distributions which are identical to the original measured data points in the uniaxial test performed along the calendering direction, i.e. direction 3, as it is shown in Figure 1 with black solid dots. Using these "experimental" distributions as initial data of the procedure detailed in Table 3 of Ref. [19] (where the functions ω_n are simply substituted by $\omega_n^\#$), the solution functions are found to be $\omega_1^\#(E) = \omega_3^\#(E)$, with the transverse strain distribution $E_2(E_1) = -E_1/2$

11

$(\nu_{12} = 1/2)$ computed also as a part of the solution. Clearly, the solution converges to the corresponding isotropic solution. That is, considering the relations $\omega_n^{\#}(E) = \omega(E) + \omega_n(E)$, $n = 1, 3$, we deduce

$$\omega_n^{\#}(E) = \omega(E); \quad \omega_n(E) = 0 \qquad (22)$$

These results indicate that the model given in Eqs. (20)–(21) has also isotropic material-symmetry congruency from a numerical point of view, as one would expect. The stress predictions in both directions provided by the computed model are also shown in Figure 1. A strictly exact fit of the experimental data is attained, as it should occur within the isotropic context (cf. Refs. [20] and [19]).

3.2. Model of Itskov and Aksel [1]

Regarding the Itskov-Aksel work of Ref. [1], the orthotropic model provided therein in terms of generalized invariants, namely Eq. (58) of that reference, includes the isotropic generalized Mooney-Rivlin model, Eq. (68) of the same reference, as a particular case. Hence, the proposed strain energy function has *theoretical* material-symmetries congruency. However, when certain slightly transversely isotropic, nearly isotropic, materials are characterized with the parameter identification procedure detailed in their work, the tendency to the Mooney-Rivlin formulation may not be observed. Furthermore, when two identical stress-strain distributions are used to initialize the parameter identification process, i.e. pure isotropic behavior is prescribed, several specific transversely isotropic solutions are found to be more optimum (in a least-squares sense) than the isotropic solution. This is due to the fact

12

that the optimization process employed to identify the material parameters does not ensure that their limit values for an isotropic material are obtained. This fact manifests that the Itskov-Aksel formulation, as given in their paper, does not have material-symmetries congruency from a *numerical* point of view.

In order to show this unexpected result, the transversely isotropic incompressible model by Itskov and Aksel, namely Eq. (95) of Ref. [1]

$$
\mathcal{W} = \frac{1}{4}\sum_{r=1}^{3}\mu_r \left\{ \frac{1}{\alpha_r}\left[\left(\sum_{i=1}^{3}w_i^{(r)}\lambda_i^2\right)^{\alpha_r} - 1\right] + \frac{1}{\beta_r}\left[\left(\sum_{i=1}^{3}w_i^{(r)}\lambda_i^{-2}\right)^{\beta_r} - 1\right]\right\}
\tag{23}
$$

where μ_r, α_r, β_r and $w_i^{(r)}$ are material parameters, along with the symmetry relations in Eq. (98) of the same Reference, i.e.

$$
w_2^{(r)} = w_3^{(r)} = \frac{1}{2}\left(1 - w_1^{(r)}\right), \quad r = 1, 2, 3
\tag{24}
$$

are employed to characterize the isotropic material of the preceding example using the minimization procedure detailed in Ref. [1]. A standard least squares curve-fitting algorithm (specifically, the Matlab function *lsqcurvefit*) has been used to fit the two point distributions shown in Figure 1 using Eqs. (100)–(102) of Ref. [1]. The optimization procedure has been initialized with the set of material parameters given in Ref. [1], i.e. Eq. (104), and the principal stretches in the calendering direction $\lambda_1^{(j)}$ ($j = 1, ..., m$) for the uniaxial test in the transversely isotropic direction 2 obtained as solution of their parameter identification procedure (note that in this example we are using the index numbering of Ref. [1], which is different from the one used in

13

the preceding example). All these material parameters and stretches initially correspond to a transversely isotropic behavior. In this first attempt to assess the numerical material-symmetries congruency of the model, the values of the parameters which have been found as "best" solution using these initial values are given in Table 1. The fact that $w_1^{(r)} \neq 1/3$, $r = 1, 2, 3$ indicates that the computed solution has not converged to the associated isotropic solution (cf. Eqs. (67) and (98) in Ref. [1]). In Figure 2, it can be observed that the stresses predicted by the model defined with the parameters given in Table 1 reproduce the tendency of the "experimental" data, although little differences between both curves (due to the lack of isotropy) are observable.

$\mu_1 = 3.84 \times 10^{-3}\,\mathrm{MPa}$	$w_1^{(1)} = 0.900$	$\alpha_1 = 4.27$	$\beta_1 = 9.44$
$\mu_2 = 2.03 \times 10^{-3}\,\mathrm{MPa}$	$w_1^{(2)} = 0.0$	$\alpha_2 = 6.84$	$\beta_2 = 7.78$
$\mu_3 = 5.44\,\mathrm{MPa}$	$w_1^{(3)} = 0.323$	$\alpha_3 = 1.0$	$\beta_3 = 1.59$

Table 1: Computed material parameters for the transversely isotropic model of Ref. [1] corresponding to the first approach in Figure 2. Initial guess (associated to a transversely isotropic material) obtained from Ref. [1].

Clearly, the foregoing solution for the set of material parameters being investigated corresponds to the nearest local minimum to the initial values given in Eq. (104) of Ref. [1]. Obviously, a local solution of any optimization procedure is strongly affected by the initial numerical values given to the unknowns of the optimization problem. Hence, one may arguably think that the isotropic limit solution could be obtained if another, more appropriate, set of initial values nearer to the isotropic solution is taken. In a second attempt to assess the numerical material-symmetries congruency of the model, we have previously obtained the values of the nine material parameters μ_r, α_r
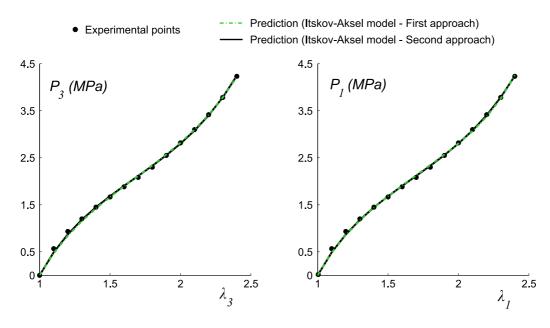
Figure 2: Nominal stresses P_3 and P_1 in terms of the stretches λ_3 and λ_1, respectively, from both uniaxial tests (black solid dots) performed on a transversely isotropic material in a hypothetical limit of isotropic behavior and predictions obtained with the model of Itskov and Aksel, Ref [1], with two different sets of material parameters. Original experimental data is obtained from the test in calendering direction from Diani et al [23]. Index numbering is consistent with Figure 1.

and β_r, $r = 1, 2, 3$, of the isotropic model (with $w_1^{(r)} = 1/3$, $r = 1, 2, 3$) which best fit one of the two identical experimental distributions of Figure 1. For this fist step, the experimental data points have been fitted by means of Eq. (100) of Ref. [1] (with $w_1^{(r)} = 1/3$). The values of the parameters which have been found as "best" solution for the isotropic model are given in Table 2. These values provide a very good agreement of the isotropic model with the experimental data.

$\mu_1 = 2.30 \times 10^{-1}\,\mathrm{MPa}$	$\alpha_1 = 4.495$	$\beta_1 = 1.004$
$\mu_2 = 2.46 \times 10^{-3}\,\mathrm{MPa}$	$\alpha_2 = 4.338$	$\beta_2 = 9.017$
$\mu_3 = 5.39\,\mathrm{MPa}$	$\alpha_3 = 1.003$	$\beta_3 = 1.0$

Table 2: Material parameters of the isotropic model of Ref. [1] computed by means of the fitting of the experimental data (only one curve) of Figure 2.

Subsequently, as before, we have proceeded to fit the two point distributions of Figure 1 using Eqs. (100)–(102) of Ref. [1]. In this second step, the optimization procedure has been initialized with the computed material parameters given in Table 2 together with the values $w_1^{(r)} = 1/3$, $r = 1, 2, 3$, and the principal stretches $\lambda_1^{(j)} = (\lambda_2^{(j)})^{-1/2}$ $(j = 1, ..., m)$, which initially describe an isotropic model. Again, a solution corresponding to a transversely isotropic description of the model, i.e. with $w_1^{(r)} \neq 1/3$, $r = 1, 2, 3$, is found to be the "best" solution for the considered initial values, see Table 3. In Figure 2, no noticeable differences are observable between the stress distributions predicted by the model in both directions. However, this is just an *apparent* isotropic response of the model in a specific situation (which has been intentionally fitted). We want to emphasize that in other more generic situations an isotropic mechanical response of the material will not be guaranteed if

16

the (transversely isotropic) model defined with the constants in Table 3 is used. Finally, we have shown that this model, even though having theoretical material-symmetries congruency, this congruency is not observed in practice using the parameter identification procedure.

$\mu_1 = 2.16 \times 10^{-1}\,\text{MPa}$	$w_1^{(1)} = 0.310$	$\alpha_1 = 4.354$	$\beta_1 = 1.0$
$\mu_2 = 2.79 \times 10^{-3}\,\text{MPa}$	$w_1^{(2)} = 0.0$	$\alpha_2 = 4.663$	$\beta_2 = 8.523$
$\mu_3 = 5.39\,\text{MPa}$	$w_1^{(3)} = 0.336$	$\alpha_3 = 1.0$	$\beta_3 = 1.0$

Table 3: Computed material parameters for the transversely isotropic model of Ref. [1] corresponding to the second approach in Figure 2. Initial guess (associated to an isotropic material) given in Table 2 along with $w_1^{(r)} = 1/3$ ($r = 1, 2, 3$) and $\lambda_1^{(j)} = (\lambda_2^{(j)})^{-1/2}$ ($j = 1, ..., m$).

At this point, we note that, besides to the lack of numerical isotropic material-symmetries congruency of this model, the optimization procedure has resulted to be strongly dependent on the initial values given to the material parameters. Hence, it is convenient that the material parameters of a model have a clear physical meaning that facilitates the task of assigning proper initial values. This fact is also encountered in isotropic materials [26].

Similar results are obtained if the two "experimental" discrete stress-stretch distributions are assumed to be equal to the original measured data points in the uniaxial test performed along the transverse direction, as it is shown in Figure 3.

Again, the solution for the spline model is such that $\omega_1^{\#}(E) = \omega_3^{\#}(E) = \omega(E)$ and $E_2(E_1) = -E_1/2$. That is, the transversely isotropic contribution $\mathcal{W}_{tr}(\boldsymbol{E}, \boldsymbol{a}_0)$ in Eq. (20) vanishes and the model converges to the corresponding isotropic solution. The *exact* predictions of the prescribed data points provided by the computed isotropic limit model are shown in Figure 3.
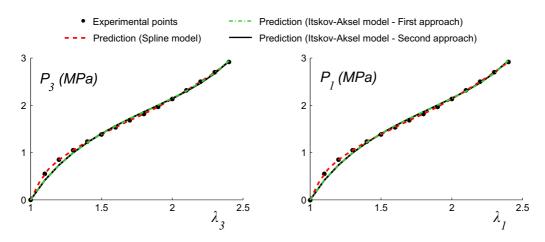
17

Figure 3: Nominal stresses P_3 and P_1 in terms of the stretches λ_3 and λ_1, respectively, from both uniaxial tests (black solid dots) performed on a transversely isotropic material in another hypothetical limit of isotropic behavior. Predictions obtained with the spline-based model and the Itskov-Aksel model of Ref. [1] with two different sets of material parameters. Original experimental data is obtained from the test in transverse direction from Diani et al [23]. Index numbering is consistent with previous Figures.

In that Figure, we also represent the predictions given by the Itskov-Aksel model with two different "best" solutions for the material parameters being investigated. The first set of them (first approach) corresponds to the transversely isotropic solution given in Table 4. These material parameters have been computed with the optimization procedure detailed in their work using as initial values the results provided by these authors in Ref. [1], i.e. Eq. (104) and the associated principal stretches $\lambda_1^{(j)}$ ($j = 1, ..., m$) for the test in the isotropic direction 2. A second set of transversely isotropic material parameters (second approach) are provided in Table 5. In this case, these material parameters have been obtained using as initial data the values $w_1^{(r)} = 1/3$, $r = 1, 2, 3$, the stretches $\lambda_1^{(j)} = (\lambda_2^{(j)})^{-1/2}$, $j = 1, ..., m$, and the associated isotropic material parameters previously computed to fit only one

18

of the two stress-stretch distributions in Figure 3 using Eq. (100) of Ref. [1] along with $w_1^{(r)} = 1/3$ (see Table 6). Again, we deduce from Tables 4 and 5 that numerical convergence to the values of the associated isotropic model is not attained in any case, even though *apparent* isotropic predictions are certainly observable in Figure 3.

$\mu_1 = 3.22 \times 10^{-4}\,\text{MPa}$	$w_1^{(1)} = 0.0$	$\alpha_1 = 6.94$	$\beta_1 = 1.0$
$\mu_2 = 1.17 \times 10^{-3}\,\text{MPa}$	$w_1^{(2)} = 0.136$	$\alpha_2 = 7.18$	$\beta_2 = 11.1$
$\mu_3 = 4.77\,\text{MPa}$	$w_1^{(3)} = 0.330$	$\alpha_3 = 1.0$	$\beta_3 = 1.0$

Table 4: Computed material parameters for the transversely isotropic model of Ref. [1] corresponding to the first approach in Figure 3. Initial guess (associated to a transversely isotropic material) obtained from Ref. [1].

$\mu_1 = 1.26 \times 10^{-3}\,\text{MPa}$	$w_1^{(1)} = 0.0$	$\alpha_1 = 6.35$	$\beta_1 = 1.0$
$\mu_2 = 1.82 \times 10^{-3}\,\text{MPa}$	$w_1^{(2)} = 0.237$	$\alpha_2 = 6.37$	$\beta_2 = 12.4$
$\mu_3 = 4.75\,\text{MPa}$	$w_1^{(3)} = 0.334$	$\alpha_3 = 1.0$	$\beta_3 = 1.0$

Table 5: Computed material parameters for the transversely isotropic model of Ref. [1] corresponding to the second approach in Figure 3. Initial guess (associated to an isotropic material) given in Table 6 along with $w_1^{(r)} = 1/3$ ($r = 1, 2, 3$) and $\lambda_1^{(j)} = (\lambda_2^{(j)})^{-1/2}$ ($j = 1, ..., m$).

$\mu_1 = 1.15 \times 10^{-3}\,\text{MPa}$	$\alpha_1 = 6.73$	$\beta_1 = 1.01$
$\mu_2 = 3.80 \times 10^{-3}\,\text{MPa}$	$\alpha_2 = 6.72$	$\beta_2 = 13.1$
$\mu_3 = 4.76\,\text{MPa}$	$\alpha_3 = 1.0$	$\beta_3 = 1.0$

Table 6: Material parameters of the isotropic model of Ref. [1] computed by means of the fitting of the experimental data (only one curve) of Figure 3.

3.3. Model of Holzapfel et al. [18]

Other types of strain energy functions widely encountered in the literature are based on the notion of structural tensors and integrity basis, see Ref. [27]. For an incompressible transversely isotropic hyperelastic material, the isochoric strain energy function is then formulated in terms of the following four invariants

$$I_1 = \boldsymbol{C} : \boldsymbol{I} \qquad I_2 = \frac{1}{2} \left[(\boldsymbol{C} : \boldsymbol{I})^2 - \boldsymbol{C}^2 : \boldsymbol{I} \right] \tag{25}$$

$$I_4 = \boldsymbol{C} : \boldsymbol{A}_0 \qquad I_5 = \boldsymbol{C}^2 : \boldsymbol{A}_0 \tag{26}$$

where $\boldsymbol{C}$ is the isochoric Cauchy-Green deformation tensor (i.e. $\det(\boldsymbol{C}) = I_3 = 1$) and $\boldsymbol{A}_0 = \boldsymbol{a}_0 \otimes \boldsymbol{a}_0$ is the structural tensor associated to the anisotropic direction $\boldsymbol{a}_0$. Hence, in the most general case $\mathcal{W} = \mathcal{W}(I_1, I_2, I_4, I_5)$, where coupling terms between the four invariants may be present in the expression of $\mathcal{W}$. In biomechanics, it is convenient to split the strain energy function into a part $\mathcal{W}_{is}$ associated with isotropic deformations and a part $\mathcal{W}_{anis}$ associated with anisotropic deformations [28]. For the case at hand, we write

$$\mathcal{W}(I_1, I_2, I_4, I_5) = \mathcal{W}_{is}(I_1, I_2) + \mathcal{W}_{tr}(I_4, I_5) \tag{27}$$

Proceeding in that way, note that Eq. (20) has been retrieved, in this case formulated in terms of $\boldsymbol{C}$, i.e.

$$\mathcal{W}(\boldsymbol{C}, \boldsymbol{a}_0) = \mathcal{W}_{is}(\boldsymbol{C}) + \mathcal{W}_{tr}(\boldsymbol{C}, \boldsymbol{a}_0) \tag{28}$$

20

so material-symmetries congruency is guaranteed for these models from a theoretical viewpoint. Eq. (27) is often simplified as (c.f. Ref. [29])

$$\mathcal{W}\left(I_1, I_4\right) = \mathcal{W}_{is}\left(I_1\right) + \mathcal{W}_{tr}\left(I_4\right) \tag{29}$$

According to Refs. [30, 31] the additive, uncoupled, decomposition given in Eq. (29) can be determined from a specific set of two experimental curves as in Ref. [11]. That is, two independent behavior "curves" are used to determine the constitutive functions $\mathcal{W}_{is}\left(I_1\right)$ and $\mathcal{W}_{tr}\left(I_4\right)$.

In the following example we show that (reduced) models of the form of Eq. (29) may also lack the isotropic material-symmetries congruency from a numerical standpoint if the parameter fitting procedure is not properly designed. As an example of Eq. (29) we take the transversely isotropic counterpart of the well-known model of Holzapfel et al. [18] (see also Ref. [32]), namely

$$\mathcal{W}\left(I_1, I_4\right) = \frac{c}{2}\left(I_1 - 3\right) + \frac{k_1}{k_2}\left(\exp\left(k_2\left(I_4 - 1\right)^2\right) - 1\right) \tag{30}$$

This model is specifically intended for describing the mechanical behavior of arterial walls, representing a simple starting point to model this type of materials. However, one would expect that if two equal experimental data points representations (obtained from a material tested in different directions, as in the previous example) are used to determine the model constants c, k_1 and k_2, then k_1 should strictly vanish. This is, indeed, what we define as *numerical* material-symmetries congruency.

Following an analogous procedure to that of the previous example, we

21

have tried to fit the nominal stresses given by the model Eq. (30) to the modified, purely isotropic, experimental data of Figure 1. For isochoric deformations $\lambda_1 \lambda_2 \lambda_3 = 1$. Aside, for a uniaxial test performed in direction 1, $\lambda_2 = \lambda_3$ if the plane $2-3$ is isotropic, so $\lambda_3 = \lambda_1^{-1/2}$. We have assumed an initial isotropic behavior for the initial guess values of the parameters, i.e. for example

$$c = 1\,\text{MPa} \quad \text{and} \quad k_1 = k_2 = 0 \tag{31}$$

along with the principal stretches in the "anisotropic" direction $\lambda_3 = \lambda_1^{-1/2}$ for the uniaxial test performed over the isotropic direction (denoted herein as axis 1). We note that the first partial derivative of $\mathcal{W}(I_1, I_4)$ with respect to I_4 is given by

$$\frac{\partial \mathcal{W}(I_1, I_4)}{\partial I_4} = 2k_1 (I_4 - 1) \exp\left(k_2 (I_4 - 1)^2\right) \tag{32}$$

so the initial specification $k_2 = 0$ gives no evaluation problems in the derived stress expressions. In order to fit the stress predictions of the model to the two point distributions $P_1(\lambda_1)$ and $P_3(\lambda_3)$ given in Figure 1, the Matlab function *lsqcurvefit* has been employed. The objective function has been defined as for the previous example. The solution for the material constants that have been computed in this case are

$$c = 1.659\,\text{MPa} \ , \quad k_1 = 1.024 \times 10^{-4}\,\text{MPa} \quad \text{and} \quad k_2 = 0.211 \tag{33}$$

Moreover, as a result of the parameter identification procedure, the obtained prediction for every "experimental" point (j) is also such that $\lambda_3^{(j)} \neq$

22

$(\lambda_1^{(j)})^{-1/2}$ for the uniaxial test performed over the "isotropic" direction. From these results, it is apparent that the numerical procedure has not converged to the corresponding isotropic solution included in the model given in Eq. (30) because we have obtained $\mathcal{W}_{tr}(I_4) \neq 0$. In Figure 4 it can be observed the *different* responses predicted by the model over the two *isotropic* directions, respectively. We want to emphasize that the fact that k_1 is rather small, in relative terms (when compared to the isotropic material constant c), causes that the isotropic behavior is dominant for moderate stretches in both directions (so it is numerically congruent for moderately large strains). However, for larger values of λ the anisotropic contribution becomes dominant for the test in the "anisotropic" direction, which causes the response to be different from the one in the transverse isotropic direction.

Additionally, we show in Figure 5 the results obtained for the fitting of this model to the two first Piola-Kirchhoff stress distributions of Figure 3. Numerical convergence to the exact isotropic response of the model (with $k_1 = 0$) is not attained either, although better results are obtained for the range of deformations under study.

Finally, we note that in order to prevent this undesired issue (specially when slightly anisotropic, nearly isotropic materials are characterized with anisotropic strain energy functions) it is possible to design a constrained parameter fitting procedure so as to attain numerical material-symmetries congruency for analytically congruent models.
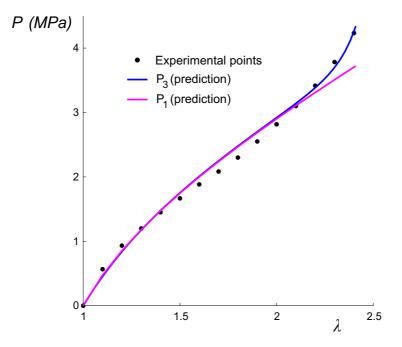
Figure 4: Nominal stresses P_3 and P_1 in terms of the stretches λ_3 and λ_1, respectively, from both uniaxial tests (black solid dots) performed on a transversely isotropic material in a hypothetical limit of isotropic behavior and predictions obtained with the model of Holzapfel et al., Ref [18], initialized with isotropic material constants. Original experimental data is obtained from the test in calendering direction from Diani et al [23].
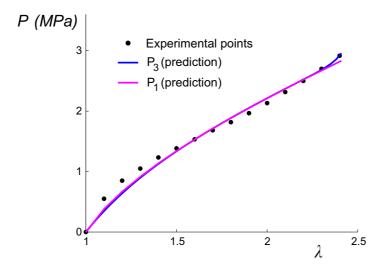
Figure 5: Nominal stresses P_3 and P_1 in terms of the stretches λ_3 and λ_1, respectively, from both uniaxial tests (black solid dots) performed on a transversely isotropic material in another hypothetical limit of isotropic behavior. Predictions obtained with the model of Holzapfel et al., Ref [18], initialized with isotropic material constants. Original experimental data is obtained from the test in transverse direction from Diani et al [23].

4. Conclusions

In this paper we have presented the material-symmetries congruency property for anisotropic hyperelastic materials. This is a desirable material property for several reasons. For example, it guarantees that the isotropic behavior of the matrix is recovered when the volume of reinforcement vanishes, as one should expect. It also guarantees for orthotropic materials that when the volume of one of the fibers vanishes, the transversely isotropic behavior is recovered.

The material-symmetries congruency property is not only an analytical issue, it is also a numerical one. The lack of numerical material-symmetries congruency in analytically congruent materials is due to the design of the parameter-fitting procedure inherent to the model from composite material

25

experiments. The use of material parameters with a clear physical interpretation in the material models easies the development of procedures that preserve the material-symmetries congruency not only from an analytical but also from a numerical point of view.

Acknowledgements

References

[1] M. Itskov, N. Aksel. A class of orthotropic and transversely isotropic hyperelastic constitutive models based on a polyconvex strain energy function. International Journal of Solids and Structures, 41, 3833–48, 2004.

[2] M. Latorre, F.J. Montáns. What-You-Prescribe-Is-What-You-Get orthotropic hyperelasticity. Computational Mechanics, 53(6), 1279–1298, 2014.

[3] G.A. Holzapfel. Nonlinear Solid Mechanics. A Continuum Approach For Engineering. Wiley, Chichester, 2000.

[4] G.A. Holzapfel, R.W. Ogden. Constitutive modelling of passive myocardium. A structurally-based framework for material characterization. Philosophical Transactions of the Royal Society of London, Series A, 367, 3445–3475, 2009.

[5] S. Göktepem S.N.S. Acharya, J. Wong, E. Kuhl. Computational modeling of passive myocardium. International Journal for Numerical Methods in Engineering, 27, 1–12, 2011.

[6] J. Schröder, P. Neff, D. Balzani. A variational stable anisotropic hyperelasticity. International Journal of Solids and Structures, 42, 4352–4371, 2005.

[7] M.P. Nash, P.J. Hunter. Computational mechanics of the heart. Journal of Elasticity, 61, 113–141, 2000.

[8] D. Tang, C. Yang, T. Geva, R. Rathod, H. Yamauchi, V. Gooty, A. Tang, M.H. Kural, K.L. Billiar, G. Gaudette, P.J. del Nido. A multiphysics modeling approach to develop right ventricle pulmonary valve replacement surgical procedures with a contracting band to improve ventricle ejection fraction. Computers & Structures, 122, 78–87, 2013.

[9] C.O. Horgan, J.G. Murphy. Simple shearing of soft biological tissues. Proceedings of the Royal Society of London, Series A, 467, 760–777, 2010.

[10] K. Costa, J. Holmes, A. McCulloch. Modelling cardiac mechanical properties in three dimensions. Philosophical Transactions of the Royal Society of London, Series A, 359, 1233–1250, 2001.

[11] T. Gasser, R.W. Ogden, G.A. Holzapfel. Hyperelastic modelling of arterial layers with distributed collagen fibre orientations. Journal of the Royal Society Interface, 3, 13–35, 2006.

[12] H. Schmid, P. O'Callagan, M.P. Nash, W. Lin, I.J. LeGrice, B.H. Smaill, A.A. Young,P.J. Hunter. Myocarcial material parameter estimation. A non-homogeneous finite element study from simple shear tests. Biomechanics and Modeling in Mechanobiology, 7, 161–173, 2008.

[13] S. Rossi, T. Lassila, R. Ruiz-Baier, A. Sequeira, A. Quarteroni. Thermodynamically consistent orthotropic activation model capturing ventricular systolic wall thickning in cardiac electromechanics. European Journal of Mechanics, A/Solids, 2014, in Press. DOI: 10.1016/j.euromechsol.2013.10.009.

[14] F. Vogel, S. Göktepe, P. Steinmann, E.Kuhl. Modeling and simulation of viscous electro-active polymers. European Journal of Mechanics, A/Solids, 2014, In Press. DOI: 10.1016/j.euromechsol.2014.02.001.

[15] J. Merodio, R.W. Ogden. Instabilities and loss of ellipticity in fiber-reinforced compressible non-linearly elastic solids under plane deformation. International Journal of Solids and Structures, 40, 4707–4727, 2003.

[16] J. Merodio, R.W. Ogden. Material instabilities in fiber-reinforced non-linearly elastic solids under plane deformation. Archives of Mechanics, 54, 525–552, 2002.

[17] J.E. Bischoff, E.M. Arruda, K. Grosh. Finite element simulations of orthotropic hyperelasticity. Finite Elements in Analysis and Design, 38, 983–998, 2002.

[18] G.A. Holzapfel, T. Gasser, R.W.Ogden. A new constitutive framework

for arterial wall mechanics and a comparative study of material models. Journal of Elasticity, 61, 1–18, 2000.

[19] M. Latorre, F.J. Montáns. Extension of the Sussman–Bathe spline-based hyperelastic model to incompressible transversely isotropic materials. Computers & Structures, 122, 13–26, 2013.

[20] T. Sussman, K.J. Bathe. A Model of Incompressible Isotropic Hyperelastic Material Behavior using Spline Interpolations of Tension-Compression Test Data. Communications in Numerical Methods in Engineering, 25, 53–63, 2009.

[21] C. Truesdell, W. Noll. The non-linear field theories of mechanics. Handbuch der Physik, Vol. III/3, Springer, Berlin, New York, 2004.

[22] R.W. Ogden. Nonlinear Elastic Deformations. Dover, Mineola, New York, 1997.

[23] J. Diani, M. Brieu, J.M. Vacherand, A. Rezgui. Directional model for isotropic and anisotropic hyperelastic rubber-like materials. Mechanics of Materials, 36, 313–21, 2004.

[24] L.L. Demer, F.C.P. Yin. Passive biaxial mechanical properties of isolated canine myocardium. Journal of Physiology, 339, 615–630, 1983.

[25] E.H. Twizell, R.W. Ogden. Non-linear optimization of the material constants in Ogden's stress-deformation relation for incompressible isotropic elastic materials. J. Aust. Math. Soc. 24, 424–434, 1983.

[26] R.W. Ogden, G. Saccomandi, I. Sgura. Fitting hyperelastic models to experimental data. Computational Mechanics, 34(6), 484–502, 2004.

[27] A.J.M. Spencer. Constitutive theory for strongly anisotropic solids. In: A.J.M. Spencer (ed.), Continuum Theory of the Mechanics of Fibre-Reinforced Composites, CISM Courses and Lectures No. 282, International Centre for Mechanical Sciences, Springer-Verlag, Wien, 1–32, 1984.

[28] H.W. Weizsäcker, G.A. Holzapfel, G.W. Desch, K. Pascale. Strain energy density function for arteries from different topographical sites. Biomediz. Tech., 40, 139–141, 1995.

[29] J.D. Humphrey. Cardiovascular Solid Mechanics. Cells, Tissues, and Organs. Springer, New York, 2002.

[30] J.D. Humphrey,F.C.P. Yin. On constitutive relations and finite deformations of passive cardiac tissue. Part I: A pseudo-strain energy function. Journal of Biomechanical Engineering, 109, 298–304, 1987.

[31] G.A. Holzapfel, R.W. Ogden. On planar biaxial tests for anisotropic nonlinearly elastic solids. A continuum mechanical framework. Mathematics and Mechanics of Solids, 14, 474–489, 2009.

[32] G.A. Holzapfel, R.W. Ogden. Constitutive modelling of arteries. Proc. R. Soc. A, 466, 1551–1597, 2010.

[33] K.C.Valanis, R.F.Landel. The strain-energy function of a hyperelastic material in terms of the extension ratios. Journal of Applied Physics, 38, 2997–3002, 1967.

30